Telomere shortening and metabolic compromise underlie dystrophic cardiomyopathy

Alex Chia Yu Chang[a,b,c,d], Sang-Ging Ong[d,e], Edward L. LaGory[f], Peggy E. Kraft[a,b,c], Amato J. Giaccia[f], Joseph C. Wu[d,e], and Helen M. Blau[a,b,c,d,1]

[a]Baxter Laboratory for Stem Cell Biology, Stanford University School of Medicine, Stanford University, Stanford, CA 94305; [b]Department of Microbiology and Immunology, Stanford University School of Medicine, Stanford University, Stanford, CA 94305; [c]Institute for Stem Cell Biology and Regenerative Medicine, Stanford University School of Medicine, Stanford University, Stanford, CA 94305; [d]Stanford Cardiovascular Institute, Stanford University School of Medicine, Stanford University, Stanford, CA 94305; [e]Division of Cardiology, Department of Medicine Stanford and Department of Radiology, Stanford University School of Medicine, Stanford University, Stanford, CA 94305; and [f]Division of Radiation and Cancer Biology and Center for Clinical Sciences Research, Department of Radiation Oncology, Stanford University, Stanford, CA 94305

Duchenne muscular dystrophy (DMD) is an incurable X-linked genetic disease that is caused by a mutation in the *dystrophin* gene and affects one in every 3,600 boys. We previously showed that long telomeres protect mice from the lethal cardiac disease seen in humans with the same genetic defect, dystrophin deficiency. By generating the *mdx^4cv/mTR^G2* mouse model with "humanized" telomere lengths, the devastating dilated cardiomyopathy phenotype seen in patients with DMD was recapitulated. Here, we analyze the degenerative sequelae that culminate in heart failure and death in this mouse model. We report progressive telomere shortening in developing mouse cardiomyocytes after postnatal week 1, a time when the cells are no longer dividing. This proliferation-independent telomere shortening is accompanied by an induction of a DNA damage response, evident by p53 activation and increased expression of its target gene *p21* in isolated cardiomyocytes. The consequent repression of *Pgc1α/β* leads to impaired mitochondrial biogenesis, which, in conjunction with the high demands of contraction, leads to increased oxidative stress and decreased mitochondrial membrane potential. As a result, cardiomyocyte respiration and ATP output are severely compromised. Importantly, treatment with a mitochondrial-specific antioxidant before the onset of cardiac dysfunction rescues the metabolic defects. These findings provide evidence for a link between short telomere length and metabolic compromise in the etiology of dilated cardiomyopathy in DMD and identify a window of opportunity for preventive interventions.

Duchenne muscular dystrophy | telomere | mitochondrial dysfunction | metabolic compromise | dilated cardiomyopathy

Duchenne muscular dystrophy (DMD), the most common heritable myopathic disease in humans, is the result of a mutation in the dystrophin gene located on the X-chromosome (1, 2). The dystrophin gene, which encodes a 427-kDa cytoplasmic protein that forms the dystrophin–glycoprotein complex connecting the cytoskeleton of a muscle fiber to the surrounding extracellular matrix, is required in both skeletal and cardiac muscles (1, 3). Patients with DMD typically exhibit symptoms at 3–5 y of age, with evidence of focal necrotic skeletal myofibers, muscle hypertrophy, and high levels of serum creatine kinase (4). Loss of dystrophin in cardiac tissues of patients with DMD leads to an influx of extracellular calcium, which triggers a pathological cascade of protease activation, myocyte death, necrosis, and inflammation, resulting in increased fibrosis (5, 6). Although electrocardiography can detect cardiac dysfunction in more than half of patients with DMD aged 6–10 y, early symptoms of cardiomyopathy may go undetected because of limited exercise tolerance. With advances in respiratory support, patients with DMD now typically present with cardiac failure leading to death in the second or third decade of life (7).

A major challenge hindering the development of effective therapies for DMD has been the lack of an animal model that closely recapitulates the cardiac disease seen in patients. The most commonly used Duchenne mouse model is the *mdx^4cv* mouse, which lacks functional dystrophin similar to patients with DMD, yet exhibits only a mild skeletal muscle dystrophic phenotype, and no cardiac phenotype (8, 9). We hypothesized that telomere length might account for this difference, as mice have much longer telomeres than humans (10). Telomeres are protective DNA repeat sequences that are bound and capped by shelterin proteins at the ends of chromosomes. Shortened telomeres have been correlated with disease states both in largely nonproliferative organs, such as the heart and brain (11), and in proliferative organs and diseases, such as cancer (12). However, a functional role for critically shortened telomeres in cardiac disease has not previously been elucidated. We recently found that when *mdx^4cv* mice were generated with shorter "humanized" telomeres by breeding with mice lacking the RNA component of telomerase (mTR), the skeletal muscle wasting and cardiac failure characteristic of patients with DMD were fully manifested (13, 14). Our findings were unexpected, as in contrast to skeletal muscle, in which the loss of proliferative capacity of the satellite cells leads to muscle wasting because of the inability to meet the chronic need for regeneration, the heart is a largely quiescent tissue. Adult cardiac development is characterized by low cell turnover, as shown from carbon-14 integration generated by

Significance

We have found that long telomeres protect mice from genetic cardiac diseases analogous to those found in humans, such as Duchenne muscular dystrophy (DMD). Mice lacking dystrophin, similar to patients with DMD, exhibit only mild disease. In contrast, mice that lack dystrophin and have "humanized" telomere lengths (*mdx^4cv/mTR^G2*) fully manifest both the severe human skeletal muscle wasting and cardiac failure typical of DMD. Remarkably, telomere shortening accompanies cardiac development even after cardiomyocyte division has ceased. This chronic proliferation-independent shortening in dystrophin-deficient cardiomyocytes is associated with induction of a DNA damage response, mitochondrial dysfunction, increased oxidative stress, and metabolic failure. Our findings highlight an interplay between telomere length and mitochondrial homeostasis in the etiology of dystrophic heart failure.

www.manaraa.com

nuclear bomb tests in humans (13) and by BrdU labeling in mouse hearts (14). In the cardiomyocytes of hearts of the mdx^{4cv}/mTR^{KO} mouse model of DMD, which require dystrophin to function, we observed a significant decrease in telomere length compared with controls (15). Importantly, other muscle cell types in the same cardiac tissues, vascular smooth muscle cells that do not express dystrophin, did not exhibit shortened telomeres (15). Notably, these findings were corroborated in human cardiac tissues of patients with DMD, in which cardiomyocytes had 55% the telomere length of normal individuals (15). Although these results highlighted a role for telomere shortening in the etiology of the disease, the molecular sequelae that drive DMD heart failure were not elucidated.

Here we demonstrate that chronic telomere shortening occurs during postnatal development in cardiomyocytes of the DMD mouse model (mdx^{4cv}/mTR^{KO}) in a proliferation-independent manner. Chronic shortening, in conjunction with activation of p53, resulted in reduced mitochondrial biogenesis, decreased mitochondria copy number and respiration, and increased oxidative stress in purified cardiomyocytes. Our results define a time window for therapeutic intervention and provide insights into the molecular crosstalk between telomere maintenance and metabolic homeostasis that underlies heart failure in DMD.

Results

Mouse Model of DMD. We generated dystrophic mice with "humanized" telomere lengths by breeding the mTR mice (lacking the RNA component of telomerase, known as *mTR* or *Terc*) (16) with the exon 53 dystrophin mutant mice (mdx^{4cv}), as described previously (15, 17). Our breeding scheme yields mdx^{4cv}/mTR^{KO} double knockouts with a genetic background identical to mTR^{KO} to rule out strain differences as a cause for the observed phenotypes. Because human DMD is X-linked, our studies were restricted to male mice, and comparisons were performed using mice of all genotypes at the same age and generation (second generation; G2). G2 is well before the telomere shortening observed ubiquitously in mTR^{KO} mice with successive generations, which by G4 mimic an aging phenotype (18). To rule out the possibility of a universal aging phenotype, we assayed telomere lengths in highly proliferative tissues such as the gonads, and no shortening was observed in G2, which is in accordance with previous reports by us and others (15, 17, 19). We compared G2 double-mutant mice lacking dystrophin and *Terc* at G2 (mdx^{4cv}/mTR^{G2}) with controls of the same G2 generation: homozygous *Terc*-null mice (mTR^{G2}) and heterozygous mdx^{4cv}/mTR^{Het} mice (dystrophin-null, but expressing one allele encoding *Terc*).

DMD Hearts Exhibit Progressive Telomere Shortening and Dysfunction After Birth. Although we observed significant telomere shortening in cardiomyocytes of patients with DMD and mdx^{4cv}/mTR^{G2} mice at the onset of dilated cardiomyopathy (15), whether telomere shortening occurred acutely or chronically remained unknown. Postnatal mouse cardiomyocytes proliferate until approximately a week after birth (14, 20, 21). To determine the progression of telomere shortening during development in our DMD mouse model, we measured telomere lengths by quantitative fluorescent in situ hybridization in mdx^{4cv}/mTR^{G2}, mdx^{4cv}/mTR^{Het}, and mTR^{G2} cardiomyocytes at 1, 4, 8, and 32 weeks of postnatal age (Fig. 1 *A* and *B*). As expected, cardiomyocyte proliferation was negligible, as assessed by measuring proliferative markers such as K_i-67, phospho-Histone 3 and BrdU (Figs. S1–S3). During this nonproliferative period of cardiac development (1–32 wk), mdx^{4cv}/mTR^{G2} cardiomyocytes exhibited a significantly greater telomere-shortening relative mdx^{4cv}/mTR^{Het} and mTR^{G2} (37.6% vs. 20.7% and 23.3%, respectively) (Fig. 1*C*). These data suggest that dystrophin deficiency exacerbates proliferation-independent telomere shortening in mdx^{4cv}/mTR^{G2} animals.
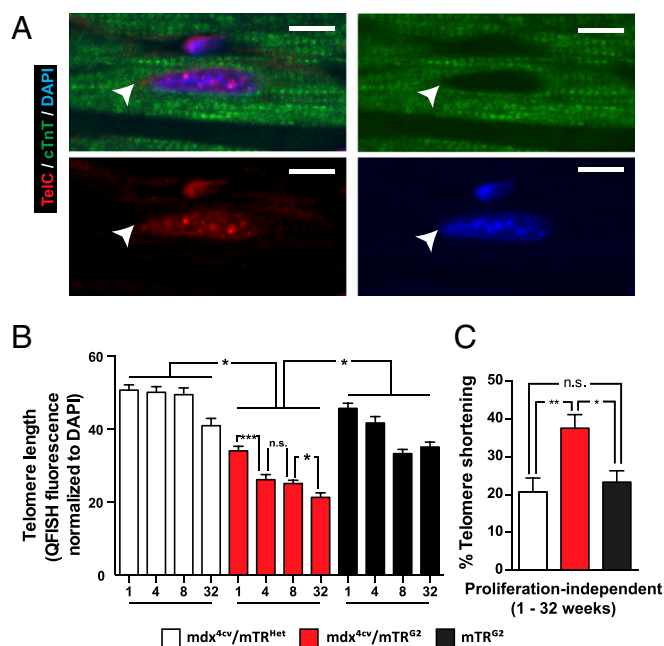
Fig. 1. Dystrophin-deficient cardiomyocytes exhibit progressive telomere shortening in two phases: proliferation dependent and proliferation independent. (*A*) Telomere length (TelC) was evaluated by immunofluorescence staining relative to DAPI staining in cardiac troponin T–positive cardiomyocytes. White arrowheads indicate nuclei within a cardiomyocyte from a mdx^{4cv}/mTR^{G2} animal. (*B*) Intensity of telomere staining relative to DAPI of cardiomyocytes is shown for 1-, 4-, 8-, and 32-wk-old hearts (n = 3 per genotype). The number of nuclei (N) scored was mdx^{4cv}/mTR^{Het} (n = 560, 318, 475, and 353), mdx^{4cv}/mTR^{G2} (n = 558, 292, 370, and 284), and mTR^{G2} (n = 513, 287, 419, and 349) for 1-, 4-, 8-, and 32-wk-old hearts, respectively. (*C*) Percentages of telomere shortening are shown for preadult (1 vs 8 wk old), adult phases (8 vs 32 wk old), and proliferation-independent phase (1 vs 32 wk old). (Scale bars, 10 μm.) Data are represented as mean ± SEM. Statistical analyses entailed nonparametric Kruskal-Wallis test corrected with Dunn's multiple comparisons test. *P < 0.05; **P < 0.01; ***P < 0.001.

We sought to determine whether telomere shortening in cardiomyocytes lacking dystrophin was accompanied by a loss of shelterin proteins that protect telomeres (22). In Langendorff-isolated cardiomyocytes, we measured the transcript levels of shelterin proteins by RT-quantitative PCR and observed a decrease in expression levels of the telomere repeat binding protein *Trf1* and a reduction in the telomere-capping components (*Tpp1*, *Pot1a*, and *Pot1b*) in mdx^{4cv}/mTR^{G2}, but not mdx^{4cv}/mTR^{Het} or mTR^{G2}, cardiomyocytes, whereas no difference was seen in *Trf2* and *Tin2* (Fig. 2 *B–D*). Taken together, these results provide evidence that the dystrophic phenotype is associated with a reduction in expression of genes encoding telomere-capping proteins, which could exacerbate telomere shortening in cardiomyocytes.

Critically Short Telomeres Result in a DNA Damage Response. To determine whether shortened telomeres lead to a DNA damage response, we assessed the amount of the p53 binding protein 1 (53bp1). For this purpose, we performed flow cytometry on cardiomyocytes isolated from Langendorff-perfused heart preparations. Cardiomyocytes from mdx^{4cv}/mTR^{G2} mice exhibited a significantly higher percentage of 53 bp1+ cardiomyocytes compared with mdx^{4cv}/mTR^{Het} and mTR^{G2} controls (86.9 ± 2.4%, 36.4 ± 10.0%, and 27.3 ± 18.8%, respectively) (Fig. 2 *C* and *D*), indicative of an increased DNA damage response. As additional readouts of the DNA damage response, we examined the level of p53 and its downstream targets. In accordance with our

GENETICS
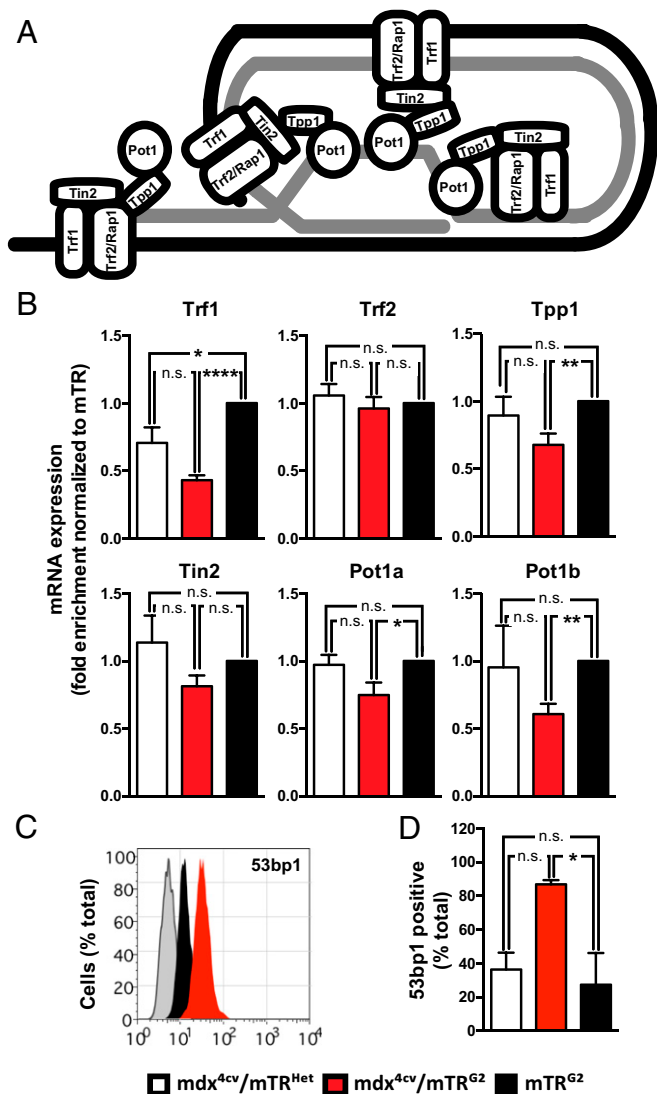
Fig. 2. Cardiomyocytes of DMD mouse model exhibit telomere dysfunction. (*A*) Schematic of telomeric ends protected by shelterin proteins. (*B*) Endogenous expression levels of telomere capping genes were determined by RT-qPCR in primary cardiomyocytes: *Trf1*, *Trf2*, *Tpp1*, *Tin2*, *Pot1a*, and *Pot1b* ($n = 4–5$ mice per genotype; technical replicates $n = 2$). (*C*) Percentage of DNA damage response marker 53bp1 positivity was quantified by flow cytometry relative to IgG control (gray). (*D*) 53bp1-positive cardiomyocytes (percentage total) are shown ($n = 3$ mice per genotype; $n = 5,000$ cardiac troponin T–positive cells per sample). All assays were performed using 8-wk-old animals. Data are represented as mean ± SEM. Statistical analyses entailed one-way ANOVA with post hoc Bonferroni correction. *$P < 0.05$; **$P < 0.01$; ****$P < 0.0001$.

53bp1 findings, p53, which is normally subjected to ubiquitination and degradation via the MDM2 complex (23), was increased in mdx^{4cv}/mTR^{G2} cardiomyocytes, evident by immunoblotting (Fig. 3*A*). In addition, we detected significant increases in the proportion of isolated cardiomyocytes expressing p53 in mdx^{4cv}/mTR^{G2} (33.7 ± 7.8%) compared with mdx^{4cv}/mTR^{Het} (5.2 ± 1.0%) and mTR^{G2} controls (7.6 ± 2.8%) by flow cytometry (Fig. 3 *B* and *C*). Induction of the p53 target gene *p21* was also evident in mdx^{4cv}/mTR^{G2} cardiomyocytes by RT-qPCR (Fig. 3*D*). The increase in *p21* transcript levels was accompanied by a twofold increase in the proportion of cardiomyocytes expressing p21 protein assayed by flow cytometry in mdx^{4cv}/mTR^{G2} compared with mdx^{4cv}/mTR^{Het} and mTR^{G2} controls (63.4 ± 11.4% vs. 22.2 ± 2.1% and 29.0 ± 8.6%, respectively) (Fig. 3 *E* and *F*).

p53 activation is known to block mitochondrial biogenesis by inhibiting expression of peroxisome proliferator-activated receptor gamma coactivator 1-alpha and 1-beta (Pgc1α and Pgc1β) (19). Accordingly, RT-qPCR assays revealed a significant decrease in *Pgc1β* transcript levels and, to a lesser extent, *Pgc1α*, in mdx^{4cv}/mTR^{G2} compared with control mdx^{4cv}/mTR^{Het} and mTR^{G2} cardiomyocytes (Fig. 3 *G* and *H*). Taken together, these data provide evidence that critically shortened telomeres in dystrophin-deficient cardiomyocytes in conjunction with a DNA damage response block mitochondrial biogenesis.

Decreased Mitochondrial Biogenesis Results in Mitochondrial Dysfunction. To evaluate the mitochondrial status of dystrophin-deficient cardiomyocytes, we analyzed mitochondrial amount, function, and ATP output in freshly isolated cardiomyocytes (Fig. 4*A*). To assess the level of mitochondrial biogenesis, we used the standard mitochondrial copy number RT-qPCR assay (24). A significant decrease in mitochondria copy number was observed in mdx^{4cv}/mTR^{G2} compared with mdx^{4cv}/mTR^{Het} and mTR^{G2} controls (Fig. 4*B*). Proteomic mass spectrometry of Langendorff isolated cardiomyocytes at 8 wk of age provided further evidence for a significant decrease in mitochondrial proteins in mdx^{4cv}/mTR^{G2} relative to control mTR^{G2} and wild-type mice
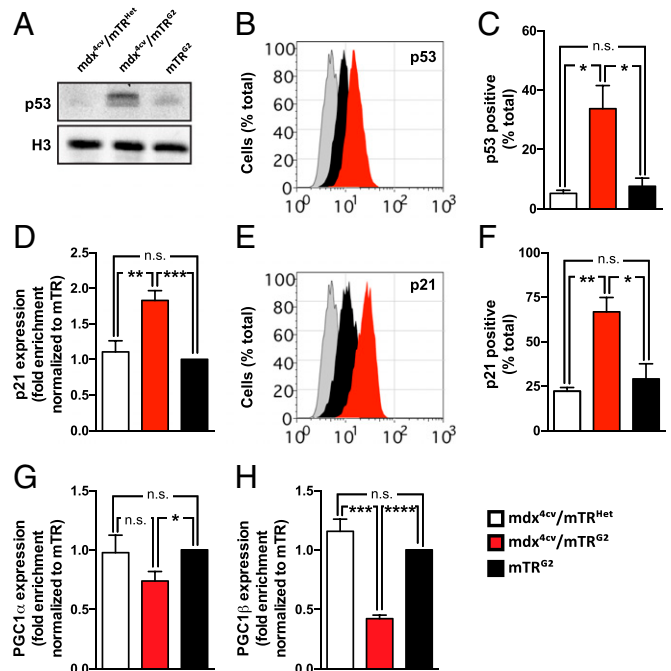
Fig. 3. Critically short telomeres lead to activation of p53, leading to decreased mitochondrial biogenesis. (*A*) Cell lysates from cardiomyocytes were immunoblotted for p53. Histone 3 (H3) protein expression was used as loading control. (*B*) Percentage of p53 positivity was quantified by flow cytometry at the population level. (*C*) Percentage of p53-positive cardiomyocytes determined by area under the curve relative to IgG control (gray; $n = 3$ mice per genotype; $n = 5,000$ cardiac troponin T–positive cardiomyocytes per condition). (*D*) Expression levels of p53 target gene, *p21*, were determined by RT-qPCR in cardiomyocytes ($n = 4–5$ mice per genotype; technical replicates $n = 2$). (*E*) p53 activation evaluated as a function of p21 protein levels by flow cytometry in cardiomyocytes. (*F*) Percentage of p21-positive cardiomyocytes determined by area under the curve relative to IgG control (gray; $n = 3$ mice per genotype; $n = 5,000$ cardiac troponin T–positive cells per sample). (*G* and *H*) Reduced expression levels of *Pgc1α and Pgc1β*, known p53 targets, determined by RT-qPCR ($n = 4–5$ mice per genotype; technical replicates $n = 2$). All assays were performed using 8-wk-old mice. Data are represented as mean ± SEM. Statistical analyses entailed one-way ANOVA with post hoc Bonferroni correction. *$P < 0.05$; **$P < 0.01$; ***$P < 0.001$; ****$P < 0.0001$.

Chang et al.
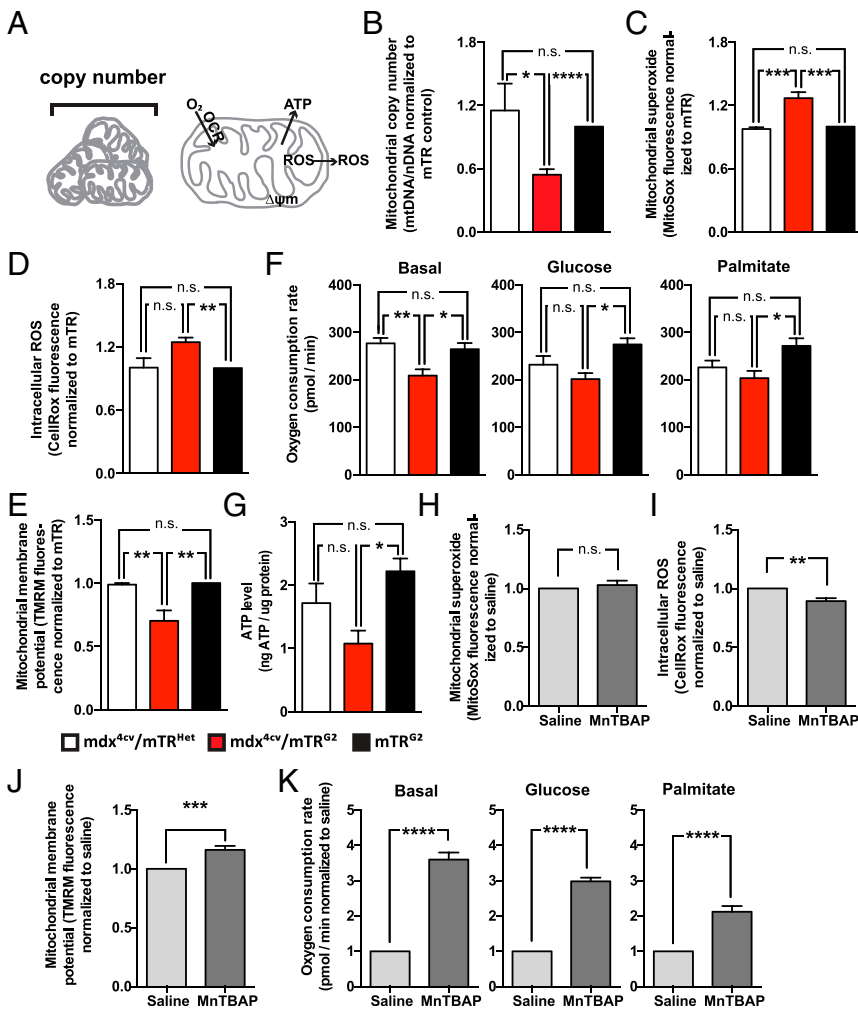
Fig. 4. Critically short telomeres result in mitochondrial dysfunction in cardiomyocytes of DMD mouse model. (*A*) Scheme for mitochondrial measurements. (*B*) Mitochondria copy number assessed as mitochondrial gene (Nd2) to nuclear DNA (Nrf1) in mdx^{4cv}/mTR^{G2}, mdx^{4cv}/mTR^{Het}, and mTR^{G2} cardiomyocytes ($n = 5$–8 mice per genotype; technical $n = 2$). (*C*) Mitochondrial superoxide species (MitoSox Red) and (*D*) intracellular reactive oxygen species (CellROX Deep Red) were measured in cardiomyocytes ($n = 4$–5 mice per genotype; technical replicates $n = 4$–5). (*E*) Mitochondrial membrane potentials (Δψm) were detected by fluorogenic probe TMRM in cardiomyocytes ($n = 4$–5 mice per genotype; technical replicates $n = 4$–5). (*F*) Real-time oxygen consumption rate was measured in freshly isolated mdx^{4cv}/mTR^{G2}, mdx^{4cv}/mTR^{Het}, and mTR^{KO} cardiomyocytes. Cells were exposed to 5 mM glucose, 167 μM Palmitate, or assay medium alone ($n = 5$ mice per genotype; technical $n = 8$). (*G*) Mean ATP levels normalized to total protein in cardiomyocyte lysates ($n = 4$–5 mice per genotype). (*H*) Mitochondrial superoxide species (MitoSox Red). (*I*) intracellular reactive oxygen species (CellROX Deep Red), (*J*) mitochondrial membrane potentials (Δψm), and (*K*) real-time oxygen consumption rate were measured in freshly isolated mdx^{4cv}/mTR^{G2} cardiomyocytes treated with either MnTBAP or saline vehicle ($n = 8$ mice per treatment; technical $n = 4$–8). All assays performed using 8-wk-old mice. Data are represented as mean ± SEM. Statistical analyses entailed one-way ANOVA with post hoc Bonferroni correction, except for the MnTBAP rescue experiments, for which a two-tailed Student's t test was used. *$P < 0.05$; **$P < 0.01$; ***$P < 0.001$; ****$P < 0.0001$.

(Fig. S4 and Dataset S1). In accordance with the development of dilated cardiomyopathy, proteins involved in muscle differentiation and muscle contraction were significantly increased, whereas proteins involved in oxidation and reduction reactions were significantly decreased in mdx^{4cv}/mTR^{G2} cardiomyocytes relative to controls.

To examine the integrity of mitochondria in dystrophic mice, isolated cardiomyocytes were assayed for intracellular reactive oxygen species (ROS), mitochondrial superoxide, and mitochondrial membrane potential. We observed a 20–30% increase in both mitochondrial superoxide and cellular ROS in mdx^{4cv}/mTR^{G2} cardiomyocytes relative to mdx^{4cv}/mTR^{Het} and mTR^{G2} controls (Fig. 4 *C* and *D*). In parallel, we observed a significant 30% decrease in mitochondrial membrane potential in mdx^{4cv}/mTR^{G2} cardiomyocytes relative to mdx^{4cv}/mTR^{Het} and mTR^{G2} controls, indicative of mitochondrial compromise (Fig. 4*E*). To evaluate mitochondrial respiration in real-time, we subjected freshly isolated cardiomyocytes to three substrate conditions: basal assay medium (no substrate), 5 μM glucose, or 167 μM palmitate. In all three conditions, mdx^{4cv}/mTR^{G2} cardiomyocytes showed a decrease in oxygen consumption rate compared with mTR^{G2} and mdx^{4cv}/mTR^{Het} controls (Fig. 4*F*). As a measure of mitochondrial output, we assayed ATP concentration in purified cardiomyocyte cell lysates. Lysates from mdx^{4cv}/mTR^{G2} cardiomyocytes exhibited a marked decrease in ATP levels compared with mdx^{4cv}/mTR^{Het} and mTR^{G2} controls (Fig. 4*G*). Together, these results suggest that DMD cardiomyocytes exhibit reduced mitochondrial biogenesis

and increased oxidative stress as a result of telomere shortening and p53 activation, culminating in metabolic compromise.

Mitochondrial Antioxidant MnTBAP Restores Mitochondrial Function. Previously, we showed that treatment of dystrophic mdx^{4cv}/mTR^{G2} animals beginning at 8 wk of age with mitochondrial-specific antioxidant manganese (III) tetrakis (4-benzoic acid) porphyrin chloride (MnTBAP) delayed the progression of dystrophic cardiomyopathy at 32 wk, as well as prolonged survival (15). To determine whether an intervention could impede the mitochondrial dysfunction observed at 8 wk of age, we subjected dystrophic mice to MnTBAP beginning at 4 wk of age. Although treatment with MnTBAP during a 4-wk period did not reduce the level of mitochondrial superoxide production, overall cellular ROS levels were reduced, and mitochondrial membrane potential was restored compared with saline-treated controls (Fig. 4 *H*–*J*). Importantly, MnTBAP treatment was sufficient to significantly abrogate the loss of mitochondrial respiration compared with saline-treated dystrophic controls. Together, these results suggest that in dystrophin-deficient cardiomyocytes, mitochondrial compromise can be partially alleviated in mdx^{4cv}/mTR^{G2} by early intervention with a mitochondrial-specific antioxidant MnTBAP.

Discussion
Our findings reveal that long telomeres protect mice from human genetic cardiomyopathies such as DMD, resolving a major conundrum. A long-term enigma has been that although the mdx

Chang et al.

www.manaraa.com

mouse lacks dystrophin, similar to patients with DMD, it does not manifest a cardiac phenotype, whereas patients succumb because of dilated cardiomyopathy. For unknown reasons, humans have much shorter telomeres than mice (10). When we "humanized" telomeres of dystrophin-deficient mdx^{4cv} mice to be similar in length to those in humans by breeding mdx^{4cv} to Terc knockout mice, the mice died prematurely as a result of dilated cardiomyopathy (15). Moreover, the severe skeletal muscle phenotype characteristic of patients with DMD was not evident in dystrophin-deficient mdx^{4cv} mice despite chronic cycles of degeneration and regeneration, because long telomeres fueled the stem cell reserve and increased the regenerative capacity of the muscle stem cells (17). Indeed, these results provide mechanistic insights into our prior studies showing that myoblasts, even from young DMD patients, have markedly impaired proliferative capacity (25). Using our mdx^{4cv}/mTR^{G2} mice, we show here that significant telomere attrition occurs during postnatal dystrophic heart development in a proliferation-independent manner. Others have shown that, loss of telomere protection due either to reduced levels of a shelterin or of the miR-34 target, PNUTS, is associated with heart disease (26, 27). Conversely, elongation of telomeres by increasing telomerase activity conferred protection in mouse hearts subjected to myocardial infarction (28). In our mdx^{4cv}/mTR^{G2} model, shortened telomeres correlated with decreased levels of three shelterins Trf1, Tpp1 and Pot1a/b. To probe cause and effect and reveal the mechanism underlying telomere shortening, an alternative is needed as the cultures of dissociated murine cardiomyocytes used here do not survive beyond 1–2 d. Of particular interest would be an elucidation of how cardiomyocyte telomeres shorten as a result of dystrophin deficiency in a proliferation-independent manner.

Telomere length is reduced in cardiomyopathy due to aging in mice and humans (11, 19). Our assessment was performed in cardiomyocytes of mouse heart tissues, as telomere length is not a reliable diagnostic marker for cardiovascular disorders when measured in the leukocytes of patients (29). Indeed, it is essential to evaluate telomere length in the relevant cell type, cardiomyocytes. This is clear from our findings which indicate that reduced telomere length is a robust indicator of cardiac dysfunction in cardiomyocytes lacking dystrophin. By contrast, other muscle cell types within the dystrophin-deficient hearts, such as smooth muscle cells of the vasculature that do not require dystrophin have normal telomere lengths. Together, these results support the hypothesis that it is the need for contraction in the absence of a crucial contractile protein, dystrophin, that leads to shortened telomeres in cardiomyocytes. Further, our findings suggest that telomere length is integral to cardiac health and suggest that interventions that delay or halt telomere erosion could be beneficial for DMD patients and the aging population at increased risk for cardiovascular disease.

Our findings also suggest the possibility that telomere shortening could be a hallmark of other genetic dilated cardiomyopathies. Accordingly, "humanizing" the telomeres of mouse models lacking other proteins essential to contraction that culminate in dilated cardiomyopathy might better recapitulate the disease phenotype seen in patients with the same genetic defect. Such "humanized" models should prove useful for gaining insights into disease etiology and progression, and for tests of therapeutic interventions.

Our detection of elevated 53bp1 and p53 in mdx^{4cv}/mTR^{G2} cardiomyocytes suggests that critically short telomeres, in conjunction with dystrophin deficiency, may be sufficient to induce a DNA damage response. Short telomeres have been shown previously to be associated with induction of 53bp1 and activation of p53 (16, 19, 22), but not in the context of genetic cardiac disease. Here we show that activation of p53 in mdx^{4cv}/mTR^{G2} cardiomyocytes leads to a marked reduction in mitochondrial

biogenesis and concomitant decreases in Pgc1α/β, membrane potential, and respiration evident at 8 wk of age, a point at which dilated cardiomyopathy is not evident by electrocardiography, echocardiogram, or MRI (15). Similarly, p53 has been implicated in $TERT^{G4}$ null mice, a mouse model of premature aging associated with ubiquitous telomere shortening resulting from the absence of the protein component of telomerase. These mice typically develop mitochondrial dysfunction because of p53-dependent inhibition of PGC1α/β and dilated cardiomyopathy at G4, but that can be prevented if the mice lack p53 as a result of genetic ablation (19). In skeletal muscle, the absence of Pgc1α leads to loss of mitochondrial integrity and remodeling, in part because of up-regulation of the mitofusion 2 (Mfn2) protein (30). Furthermore, cardiac-specific deletion of Mfn1/2 in mice results in increased mitochondrial fragmentation and lethal dilated cardiomyopathy (31). Notably, dystrophin-deficient cardiomyocytes have been shown by others to exhibit elevated ROS when subjected to mechanical stretch (32), and high ROS in nonproliferating fibroblasts has been shown to cause telomere shortening (33). Our finding that MnTBAP treatment is able to restore mitochondrial respiration (Fig. 4) and increase survival (15) suggests ameliorating mitochondrial function may improve cardiac function.

A recent report showed that dystrophin functions not only as a structural contractile protein but also regulates asymmetric skeletal muscle stem cell division (34). Here, we show that dystrophin can also protect cardiomyocytes from telomere attrition and prevent mitochondrial compromise. We also provide a molecular and metabolic characterization of dystrophic cardiomyocytes. Further, our studies reveal an interplay between telomere length and mitochondrial homeostasis that is fundamental to the etiology of DMD cardiomyopathy. Together, our data suggest that interventions that restore mitochondrial biogenesis, increase telomere-capping proteins, or induce telomere elongation may halt or delay the onset of dilated cardiomyopathy in DMD.

Materials and Methods

Mice. All protocols were approved by the Stanford University Administrative Panel on Laboratory Animal Care. C57BL6 mdx^{4cv} mice and C57BL6 mTR^{Het} mice were used to generate the double-mutant animals, as described previously (15). As the human disease is X-linked, our studies were restricted to male mice. The exact number of animals for each data set and all relevant details regarding the sample size are reported with each experiment.

Adult Cardiomyocyte Assays. Hearts were excised and used for ex vivo Langendorff perfusion to isolate mature cardiomyocytes. Isolated cardiomyocytes were used directly or allowed to attach at 37 °C to laminin (1:100 in dH₂O, Sigma, L2020) precoated black 96-well clear-bottom plates (Corning Costar, 3603) in serum-free cardiomyocyte AW medium (Cellutron, m-8034). Medium was changed after 1 h, and cells were incubated for 30 min at 37 °C with various fluorescent dyes from Life Technologies: CellROX Deep Red Reagent (C10422), MitoSOX Red Mitochondrial Superoxide Indicator (M36008), and tetramethylrhodamine, methyl ester, and perchlorate (TMRM; T-668). Signal was detected using Tecan Infinite M1000 PRO machine at the Stanford High-Throughput Bioscience Center. For mitochondrial respiration measurements, 5,000 isolated cardiomyocytes were seeded onto laminin-coated XF96 microplates under basal (XF assay medium only), glucose (5 μM glucose), or Palmitate (XF Palmitate-BSA FAO Substrate kit; Seahorse Biosciences) and assayed according to manufacturer's instructions. Intracellular ATP levels were measured using the ATP Colorimetric/Fluorometric Assay Kit (Biovision). Cardiomyocyte RNA was extracted using RNeasy Micro Kit (Qiagen), and High Capacity cDNA Reverse Transcription Kit (Life Sciences) was used to generate cDNA for RT-qPCR with various Taqman probes (Table S1). Cell lysates were collected in radioimmunoprecipitation assay buffer, and immunoblotting was performed as previously described (35).

Telomere Q-FISH and Immunofluorescence and Image Acquisition. Hearts were excised at the indicated ages and fixed overnight in 4% (vol/vol) paraformaldehyde in PBS. After progressive tissue dehydration with ethanol and xylene, the heart samples were embedded in paraffin. Cardiac paraffin

sections (5 μm) were deparaffinized in xylene and rehydrated in serial ethanol concentrations. Antigen retrieval was performed in citrate buffer (10 mmol·L⁻¹ sodium citrate at pH 6.0) for 30 min in a steam cooker. Telomere Q-FISH was performed as previously reported, using TelC probes (15). Slides were blocked with staining buffer [4% (vol/vol) calf serum/0.1%Triton X-100/PBS] and stained overnight at 4 °C with various primary antibodies: mouse K_i-67 (1:50; BD, 556003), mouse phospho-Hist3 (1:50; Cell Signaling, 9706L). After washing in blocking solution, slides were incubated with the appropriate Alexa 594 secondary antibodies (1:400; Abcam) for 1 h in the dark at room temperature. The slides were washed again with PBS, fixed in 4% (vol/vol) paraformaldehyde (PFA) for 5 min, washed with PBS, and then incubated with prediluted mouse antibody for cardiac troponin t (Abcam ab74275) for 1 h at room temperature, washed with PBS and incubated with the appropriate Alexa 488 secondary antibody (1:400; Abcam) for 1 h in the dark at room temperature. The slides were then washed with PBS, counterstained with 1 μg·mL⁻¹ DAPI solution in PBS for 5 min, washed with dH₂O, air dried, and mounted with ProLong Gold Antifade (Life Technologies). Images were captured on a Nikon Spinning Disk Confocal microscope, using the NIS-Elements program (Nikon).

Flow Cytometry. Langendorff-isolated cardiomyocytes were immediately fixed in CytoFix/CytoPerm solution (BD) for 10 min and resuspended in CytoPerm solution. For BrdU assay, mice were injected with BrdU labeling reagent (Life Technologies) 24 h before cardiomyocyte isolation. Cardiomyocytes were stained in CytoPerm solution overnight at 4 °C, with various primary antibodies: rabbit 53bp1 (1:400; Novus, NB100-304), mouse p53 (1:400; Vector Lab, VP-P956), mouse K_i-67 (1:50; BD, 556003), mouse phospho-Hist3 (1:50; Cell Signaling, 9706L), mouse BrdU (BD, 347580), and p21 (1:100; Santa Cruz Biotechnology, sc-397). All samples were analyzed on BD FACSCalibur (BD Biosciences).

Proteomics Analysis. Adult cardiomyocytes from mdx/mTR^KO and mTR^KO mice (three each) were isolated using the Langendorff isolation protocol. Cytosolic and nuclear fractions were isolated using the NE-PER extraction kit (Thermo Part No. 78833). Cell lysates were diluted to 2 mg/mL in 50 mM Hepes at pH 8.0, 0.1% SDS, and reduced with 5 mM TCEP [tris(2-carboxyethyl)phosphine] (Thermo Part No. 77720) for 1 h at 50 °C. Reduced proteins were labeled with

5–10 mM iodoTMT reagents (Thermo Part No. 90103) for 1 h at 37 °C protected from light. Excess iodoTMT reagent, salt, and detergent were removed by acetone precipitation of samples at −20 °C for 4–20 h. Proteins were then digested at 37 °C for 4 h, using trypsin (Thermo Part No. 90103), and desalted using C18 spin tips (Thermo Part No. 84850). Labeled peptides (25–100 μg) were resuspended in TBS at 0.5 μg/μL and incubated with 20–100 μL immobilized anti-TMT antibody resin (Thermo Part No. 90076) overnight with end-over-end shaking at 4 °C. After collection of the unbound sample, the resin was washed four times with 4 M Urea/TBS, four times with TBS, and four times with water. Peptides were then eluted three times with TMT Elution Buffer (Part No. 90104), frozen, and dried under vacuum before LC-MS/MS analysis. A total of 868 proteins (using a cutoff of minimum three peptides) were identified. Bioinformatic analysis was performed on both up-regulated (+1.2-fold cutoff) and down-regulated (−1.2-fold cutoff) proteins that were isolated by comparing the WT with mdx/mTR^G2 and mTR^G2 with mdx/mTR^G2 independently. Gene Ontology analysis [DAVID/EASE program (36)] was used.

Statistical Analysis. All data are shown as the mean ± SEM of multiple experiments. Statistical analyses were calculated using one-way ANOVA with post hoc Bonferroni correction, nonparametric Kruskal-Wallis test with Dunn's correction for multiple comparisons, or two-tailed Student's t test. Statistical significance was considered at *$P < 0.05$, **$P < 0.01$, ***$P < 0.001$, ****$P < 0.0001$. All statistical analyses were performed using GraphPad Prism software. Source data are shown in Dataset S2.

1. Koenig M, et al. (1987) Complete cloning of the Duchenne muscular dystrophy (DMD) cDNA and preliminary genomic organization of the DMD gene in normal and affected individuals. *Cell* 50(3):509–517.
2. Bieber FR, Hoffman EP (1990) Duchenne and Becker muscular dystrophies: Genetics, prenatal diagnosis, and future prospects. *Clin Perinatol* 17(4):845–865.
3. Hoffman EP, Monaco AP, Feener CC, Kunkel LM (1987) Conservation of the Duchenne muscular dystrophy gene in mice and humans. *Science* 238(4825):347–350.
4. Chyatte SB, Vignos PJJ, Jr, Watkins M (1966) Early muscular dystrophy: Differential patterns of weakness in Duchenne, limb-girdle and facioscapulohumeral types. *Arch Phys Med Rehabil* 47(8):499–503.
5. Allamand V, Campbell KP (2000) Animal models for muscular dystrophy: Valuable tools for the development of therapies. *Hum Mol Genet* 9(16):2459–2467.
6. Mavrogeni S, et al. (2010) Myocardial inflammation in Duchenne Muscular Dystrophy as a precipitating factor for heart failure: A prospective study. *BMC Neurol* 10:33.
7. McNally EM, Kaltman JR, Benson DW, et al; Working Group of the National Heart, Lung, and Blood Institute; Parent Project Muscular Dystrophy (2015) Contemporary cardiac issues in Duchenne muscular dystrophy. Working Group of the National Heart, Lung, and Blood Institute in collaboration with Parent Project Muscular Dystrophy. *Circulation* 131(18):1590–1598.
8. Chapman VM, Miller DR, Armstrong D, Caskey CT (1989) Recovery of induced mutations for X chromosome-linked muscular dystrophy in mice. *Proc Natl Acad Sci USA* 86(4):1292–1296.
9. Bulfield G, Siller WG, Wight PA, Moore KJ (1984) X chromosome-linked muscular dystrophy (mdx) in the mouse. *Proc Natl Acad Sci USA* 81(4):1189–1192.
10. Blasco MA (2005) Mice with bad ends: Mouse models for the study of telomeres and telomerase in cancer and aging. *EMBO J* 24(6):1095–1103.
11. Terai M, et al. (2013) Association of telomere shortening in myocardium with heart weight gain and cause of death. *Sci Rep* 3:2401.
12. Blackburn EH, Epel ES, Lin J (2015) Human telomere biology: A contributory and interactive factor in aging, disease risks, and protection. *Science* 350(6265):1193–1198.
13. Bergmann O, et al. (2009) Evidence for cardiomyocyte renewal in humans. *Science* 324(5923):98–102.
14. Soonpaa MH, Kim KK, Pajak L, Franklin M, Field LJ (1996) Cardiomyocyte DNA synthesis and binucleation during murine development. *Am J Physiol* 271(5 Pt 2): H2183–H2189.
15. Mourkioti F, et al. (2013) Role of telomere dysfunction in cardiac failure in Duchenne muscular dystrophy. *Nat Cell Biol* 15(8):895–904.
16. Blasco MA, et al. (1997) Telomere shortening and tumor formation by mouse cells lacking telomerase RNA. *Cell* 91(1):25–34.
17. Sacco A, et al. (2010) Short telomeres and stem cell exhaustion model Duchenne muscular dystrophy in mdx/mTR mice. *Cell* 143(7):1059–1071.
18. Lee HW, et al. (1998) Essential role of mouse telomerase in highly proliferative organs. *Nature* 392(6676):569–574.
19. Sahin E, et al. (2011) Telomere dysfunction induces metabolic and mitochondrial compromise. *Nature* 470(7334):359–365.
20. Li F, Wang X, Capasso JM, Gerdes AM (1996) Rapid transition of cardiac myocytes from hyperplasia to hypertrophy during postnatal development. *J Mol Cell Cardiol* 28(8):1737–1746.
21. Pasumarthi KB, Field LJ (2002) Cardiomyocyte cell cycle regulation. *Circ Res* 90(10): 1044–1054.
22. de Lange T (2005) Shelterin: The protein complex that shapes and safeguards human telomeres. *Genes Dev* 19(18):2100–2110.
23. Haupt Y, Maya R, Kazaz A, Oren M (1997) Mdm2 promotes the rapid degradation of p53. *Nature* 387(6630):296–299.
24. Evdokimovsky EV, Ushakova TE, Kudriavtcev AA, Gaziev AI (2011) Alteration of mtDNA copy number, mitochondrial gene expression and extracellular DNA content in mice after irradiation at lethal dose. *Radiat Environ Biophys* 50(1):181–188.
25. Blau HM, Webster C, Pavlath GK (1983) Defective myoblasts identified in Duchenne muscular dystrophy. *Proc Natl Acad Sci USA* 80(15):4856–4860.
26. Boon RA, et al. (2013) MicroRNA-34a regulates cardiac ageing and function. *Nature* 495(7439):107–110.
27. Oh H, et al. (2003) Telomere attrition and Chk2 activation in human heart failure. *Proc Natl Acad Sci USA* 100(9):5378–5383.
28. Bär C, et al. (2014) Telomerase expression confers cardioprotection in the adult mouse heart after acute myocardial infarction. *Nat Commun* 5:5863.
29. Guzzardi MA, Iozzo P, Salonen M, Kajantie E, Eriksson JG (2015) Rate of telomere shortening and metabolic and cardiovascular risk factors: A longitudinal study in the 1934-44 Helsinki Birth Cohort Study. *Ann Med* 47(5):499–505.
30. Adhihetty PJ, et al. (2009) The role of PGC-1alpha on mitochondrial function and apoptotic susceptibility in muscle. *Am J Physiol Cell Physiol* 297(1):C217–C225.
31. Chen Y, Liu Y, Dorn GW, 2nd (2011) Mitochondrial fusion is essential for organelle function and cardiac homeostasis. *Circ Res* 109(12):1327–1331.
32. Prosser BL, Ward CW, Lederer WJ (2011) X-ROS signaling: Rapid mechano-chemo transduction in heart. *Science* 333(6048):1440–1445.
33. Sitte N, Saretzki G, von Zglinicki T (1998) Accelerated telomere shortening in fibroblasts after extended periods of confluency. *Free Radic Biol Med* 24(6):885–893.
34. Dumont NA, et al. (2015) Dystrophin expression in muscle stem cells regulates their polarity and asymmetric division. *Nat Med* 21(12):1455–1463.
35. Chang AC, et al. (2011) Notch initiates the endothelial-to-mesenchymal transition in the atrioventricular canal through autocrine activation of soluble guanylyl cyclase. *Dev Cell* 21(2):288–300.
36. Dennis G, Jr, et al. (2003) DAVID: Database for Annotation, Visualization, and Integrated Discovery. *Genome Biol* 4(5):3.

GENETICS

Chang et al.

www.manaraa.com